Hybrid Iodobismuthates by Mechanochemical Synthesis as Pseudocapacitor Electrode Materials

Yishan Lu,[a] Caroline Kirk*[a] and Neil Robertson*[a]

Supplementary

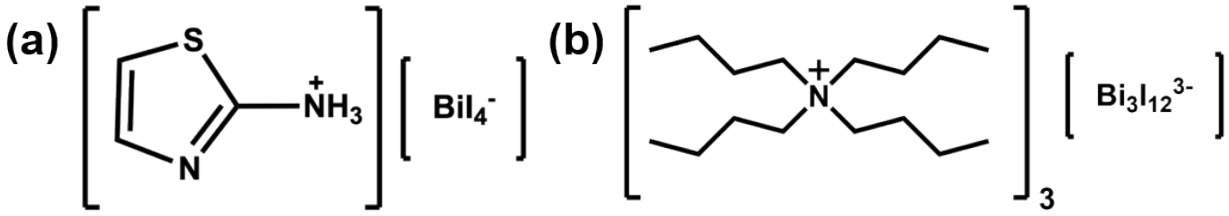

Figure S1 (a) molecular structure of [C3H5N2S][BiI4] ([AT][BiI_4]); (b) molecular structure of [(C4H9)4N]3[Bi3I12] ([TBA][BiI_3])

Table S1 CHNS elemental analysis result of ATI

Element	Expected/%	Found (1)/%	Found (2)/%
Carbon	15.81	15.59	15.55
Hydrogen	2.21	2.21	2.20
Nitrogen	12.28	12.19	12.00
Sulphur	14.06	14.96	14.71

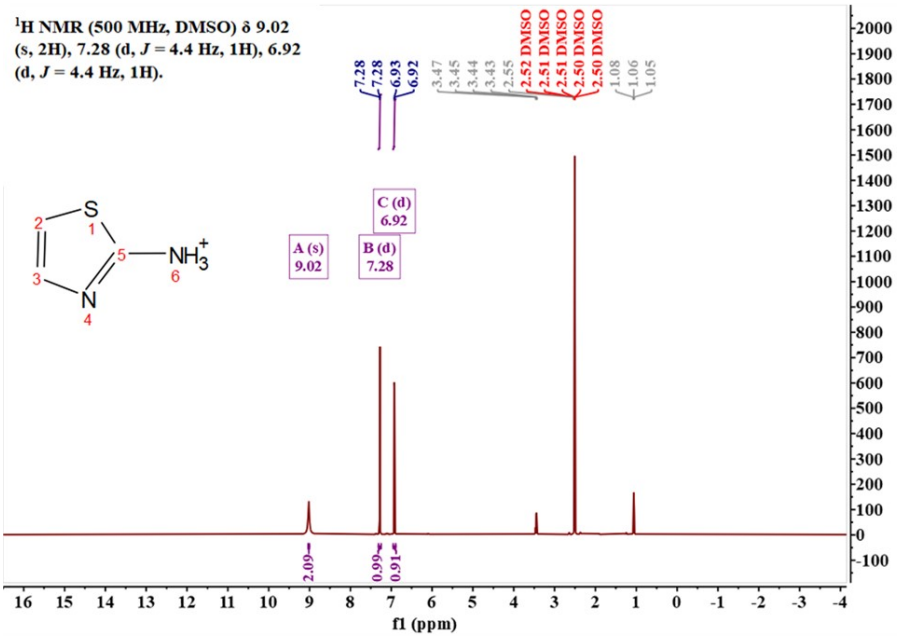

Figure S2 [1]H-NMR spectra of ATI (500 MHz, DMSO). Chemical shift (δ, ppm): 9.02 (singlet, 2H, -NH2), 7.28 (doublet, J=4.4 Hz, 1H, -N-CH=CH), 6.92 (doublet, J=4.4 Hz, 1H, -S-CH=CH).

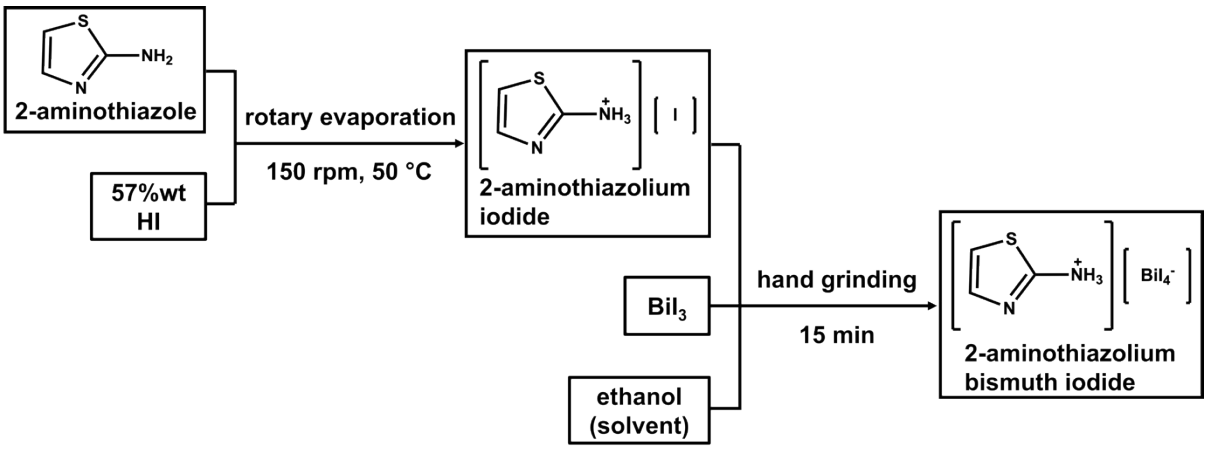

Figure S3 flow chart of ATBI synthesis. The precursor 2-aminothiazolium iodide ([AT]I) was prepared according to the reported procedure and characterised by ^{1}H-NMR (Figure S1) and CHNS elemental analysis (Table S1).

Table S2 elemental analysis result of [AT][BiI_4]

Element	Expected/%	Found (1)/%	Found (2)/%
Carbon	4.41	4.11	4.07
Hydrogen	0.62	0.53	0.53
Nitrogen	3.43	2.99	3.09
Sulphur	3.92	3.61	3.68

Table S3 ICP-MS result of [AT][BiI_4]

	Bi molecular mass ratio (%)
[AT][BiI_4] tested	28.3
[AT][BiI_4] theoretical	25.5

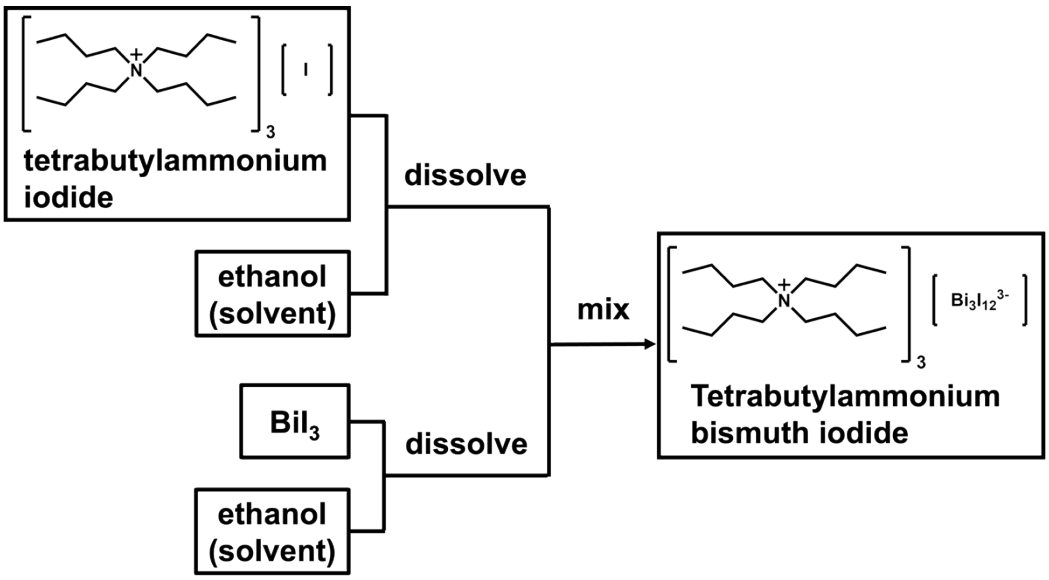

Figure S4 flow chart of $[TBA]_3[Bi_3I_{12}]$_P synthesis

Table S4 elemental analysis result of $[TBA]_3[Bi_3I_{12}]$_P

Element	Expected/%	Found (1)/%	Found (2)/%
Carbon	20.04	19.92	19.83
Hydrogen	3.75	3.81	3.82
Nitrogen	1.46	1.57	1.57
Sulphur	0	0	0

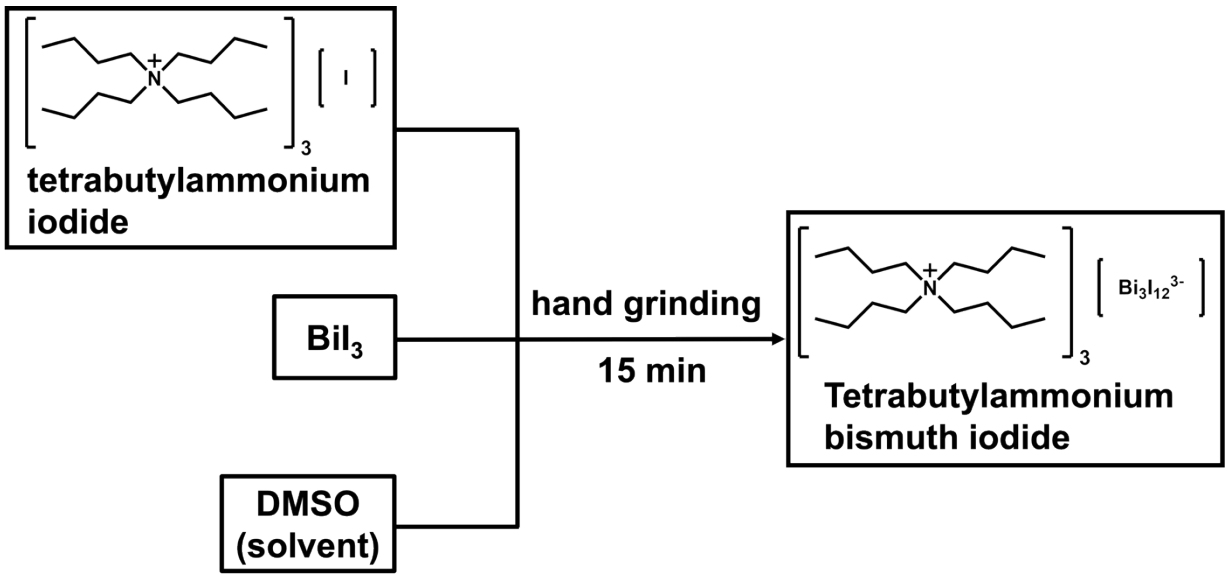

Figure S5 flow chart of $[TBA]_3[Bi_3I_{12}]$_G synthesis

Table S5 elemental analysis result of $[TBA]_3[Bi_3I_{12}]$_G

Element	Expected/%	Found (1)/%	Found (2)/%
Carbon	25.20	25.18	25.10
Hydrogen	4.76	4.99	4.96
Nitrogen	1.84	1.64	1.58
Sulphur	0	3.71	3.78

The expected result of $[TBA]_3[Bi_3I_{12}]$_P (Table S4) and $[TBA]_3[Bi_3I_{12}]$_G (Table S5) were calculated based on different assumed formula. For $[TBA]_3[Bi_3I_{12}]$_P the formula was assumed as $[TBA]_3[Bi_3I_{12}]$, because of its precipitation synthesis method and consistency with XRD result. For $[TBA]_3[Bi_3I_{12}]$_G, it was estimated using the formula $[TBA]_3[Bi_2I_9]$, which was based on the molar ratio of TBAI and BiI_3 used during synthesis. However, since the XRD result of $[TBA]_3[Bi_3I_{12}]$_G indicated the existence of monoclinic and triclinic $[TBA]_3[Bi_3I_{12}]$, we can confirm the product $[TBA]_3[Bi_3I_{12}]$ was the crystalline product obtained from the synthesis. In addition, as shown in Figure S6, the XRD pattern of $[TBA]_3[Bi_3I_{12}]$_G does not match any reported $[TBA]_3[Bi_2I_9]$ crystal structures from the database[1]. Combined with the discrepancies observed in the elemental analysis result, we suspect the presence of residual impurities in the sample, which are very likely to be amorphous and thus don't show up as strong diffraction peaks in the XRD result, instead showing as background especially in the presence of the strong $[TBA]_3[Bi_3I_{12}]$ peaks. In addition, the presence of sulphur in the result may originate from the DMSO solvent used in the synthesis, which is relatively difficult to remove.

1. C. Feldmann, *Zeitschrift für Kristallographie-New Crystal Structures*, 2001, **216**, 487–488.

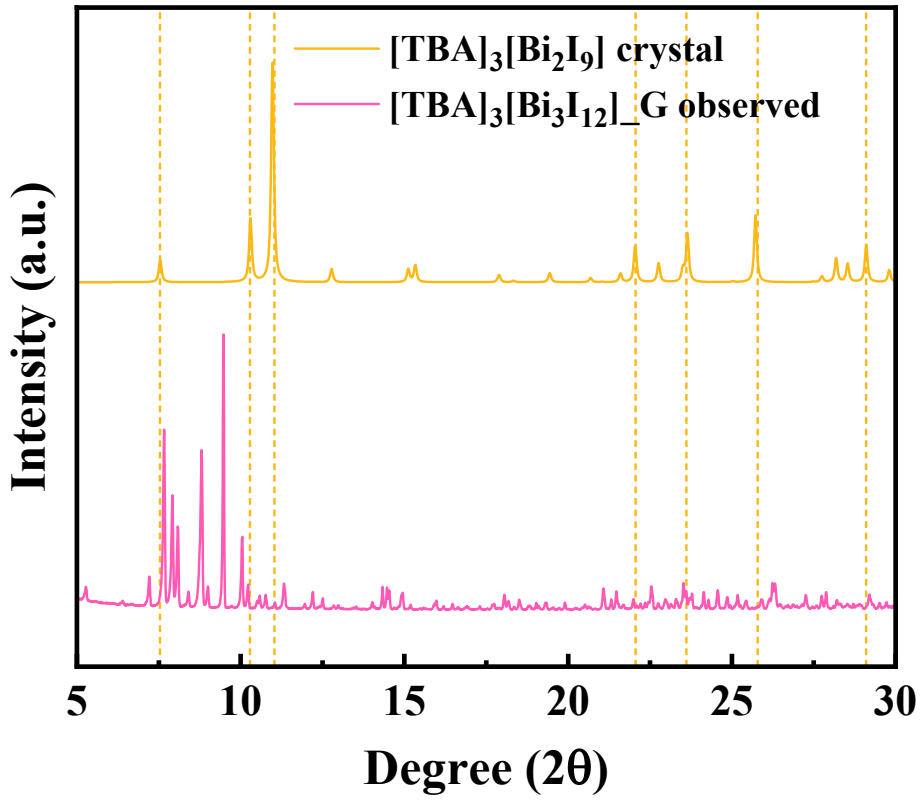

Figure S6 Theoretical PXRD pattern of the $[TBA]_3[Bi_2I_9]$ [24] (orange line) compared with the observed $[TBA]_3[Bi_3I_{12}]$_G sample (pink line).

The 1:1 molar ratio of TBAI to BiI_3 was also investigated, motivated by the goal of obtaining a purer product, since $[TBA]_3[Bi_3I_{12}]$_G was produced using a 3:2 ratio. As shown in Figure S7, however, the sample obtained from the 1:1 ratio did not match any known crystalline phase. New diffraction peaks were observed that could not be attributed to the starting materials, suggesting the formation of a potentially new $[TBAI]_x[BiI_3]_y$ phase. Further structural characterisation will be necessary to confirm this in the future. In this study, we focus on using a 3:2 molar ratio of TBAI and BiI_3 for synthesis, which yields $[TBA]_3[Bi_3I_{12}]$_G along with some organic impurities, as discussed previously, for all subsequent paragraphs.

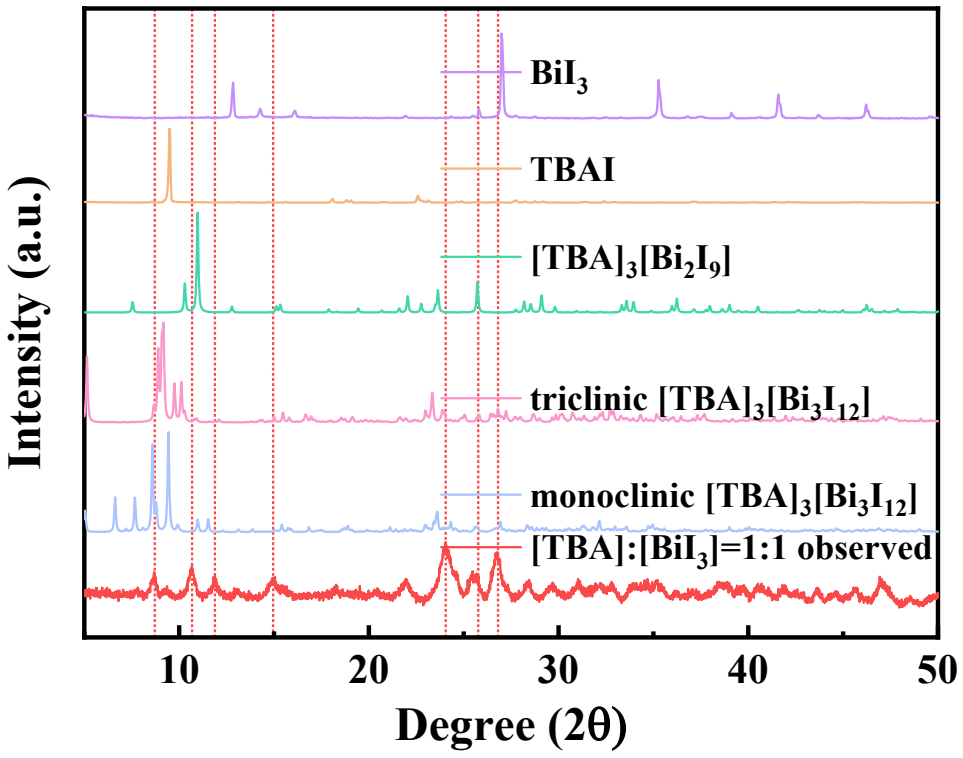

Figure S7 PXRD pattern of 1:1 TBAI and BiI_3, compared with the crystal XRD data of monoclinic and triclinic phase $[TBA]_3[Bi_3I_{12}]$ and $[TBA]_3[Bi_2I_9]$ obtained from the CSD.

Table S6 crystallographic data for [AT][BiI_4] ($C_3H_5BiI_4N_2S$), monoclinic [TBA]$_3$[Bi_3I_{12}] ($C_{36}H_{72}Bi_3I_{12}$) and triclinic [TBA]$_3$[Bi_3I_{12}] ($C_{36}H_{72}N_3Bi_3I_{12}$)

Formula	$C_3H_5BiI_4N_2S$	$C_{36}H_{72}N_3Bi_3I_{12}$	$C_{36}H_{72}N_3Bi_3I_{12}$
D_{calc}/g cm^{-3}	4.064	2.266	2.384
μ/mm^{-1}	22.546	10.61	11.219
Formula weight	819.77	2877.20	2877.20
Crystal system	Orthorhombic	Monoclinic	Triclinic
Space group	*Pbca (61)*	*$P2_1/c$*	*P 1̄ (2)*
a/Å	18.5429(4)	17.796(4)	11.9700(10)
b/Å	7.53048(19)	20.565(6)	17.5150(16)
c/Å	19.1421(6)	23.414(8)	19.5175(18)
α,β,γ/°	—	*β* = 100.25(4)	*α* = 85.426(3), *β* = 87.490(2), *γ* = *79.462(2)*
V/Å^3	2672.94	8432(4)	4008.3(6)
λ/Å	0.71073	0.71069	0.71073
T/K	120	298	150
wR_2*(all data)*	0.0803	—	—
wR_2	0.0770	—	0.0938
R_1 *(all data)*	0.0499	—	—
R_1	0.0412	0.140	0.0440

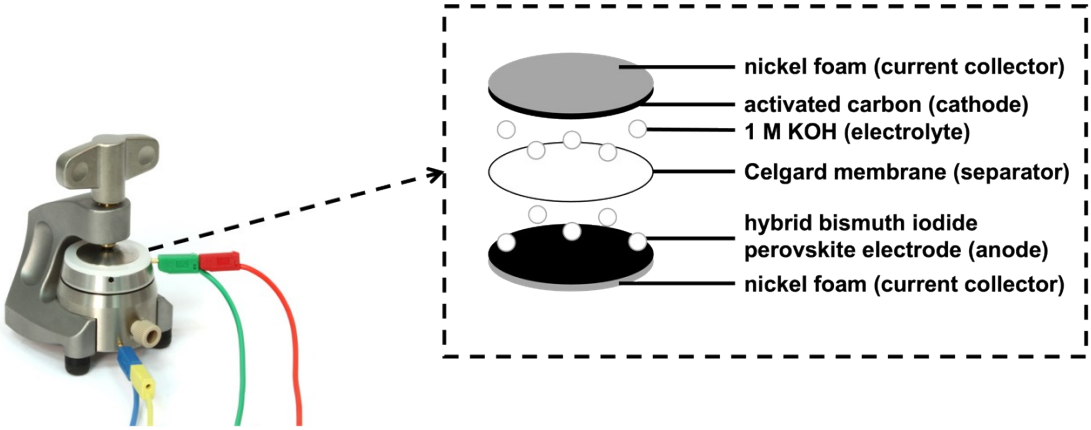

Figure S8 schematic clamp cell

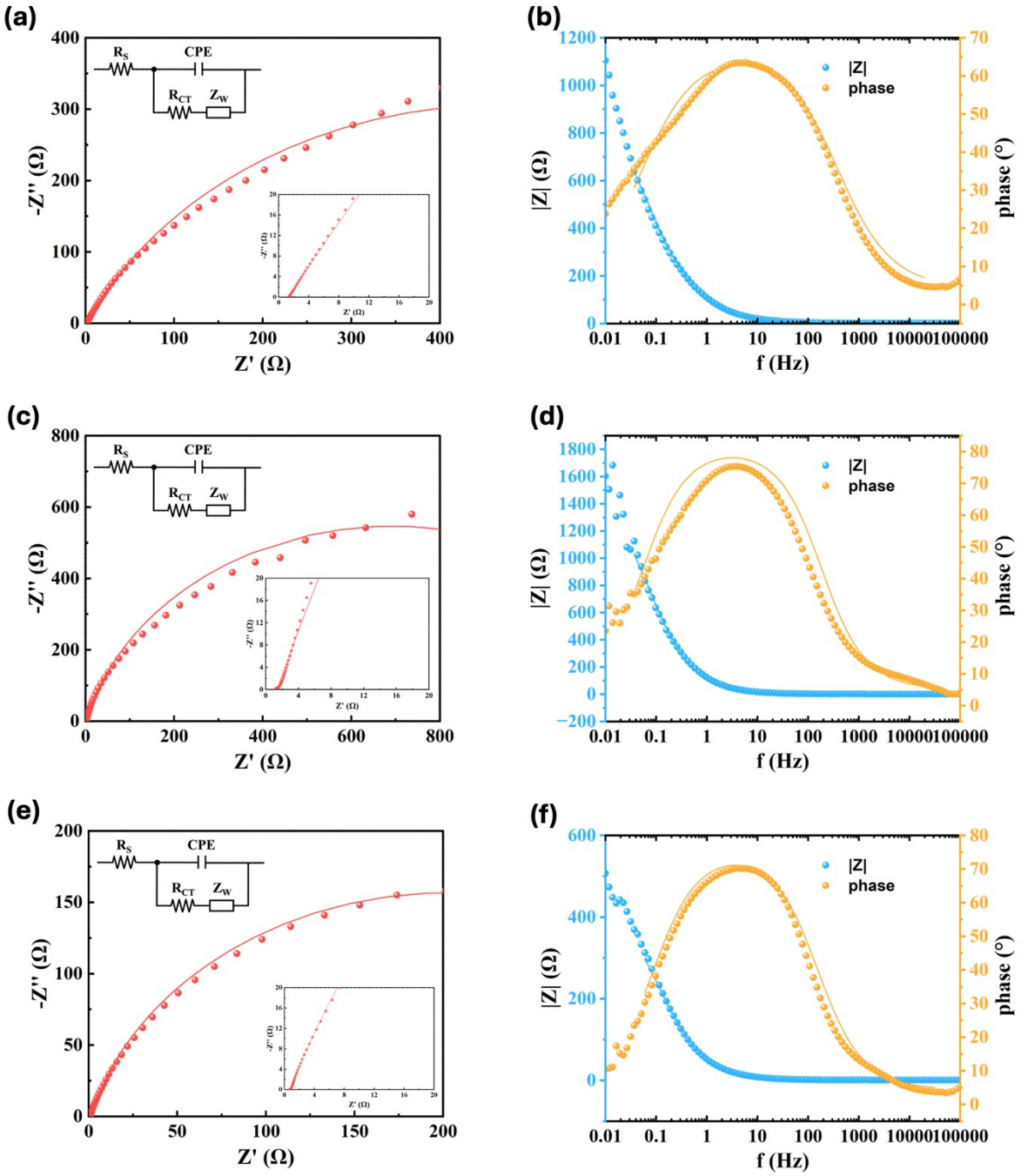

Figure S9 (a), (c), (e) Nyquist plot of $[AT][BiI_4]$, $[TBA][BiI_3]$_P and $[TBA][BiI_3]$_G electrode (red scatter) and the fitted line based on the simulated equivalent circuit diagram inserted (red line); (b), (d), (f) Bode plot of $[AT][BiI_4]$, $[TBA][BiI_3]$_P and $[TBA][BiI_3]$_G electrode electrode showing the impedance modulus (blue scattered) and the phase change (orange scattered) and the fitted line of each based on equivalent circuit (blue line and orange line). The convergence criteria χ^2 of $[AT][BiI_4]$, $[TBA]_3[Bi_3I_{12}]$_P and $[TBA]_3[Bi_3I_{12}]$_G is 0.0024, 0.016, 0.0077 which shows a fit with moderate error.

Compared with parameter C implying a pure capacitor, CPE is used to describe a nonideal capacitor caused by the inhomogeneity of electrode material surface. The difference between CPE and an ideal capacitor is described in Formula 13:

$$Z_{CPE} = 1 / (j\omega)^{\beta} Q \quad \text{(Formula 13)}$$

Where Q is the nonideal impedance of CPE, β is ideality factor ($\beta = 1$, CPE is an ideal capacitor, where $Q = C$) and CPE-Yo implies the capacitance and CPE-N is the value of β. Normally CPE-N is around 0.8 ~ 1.0.[76]

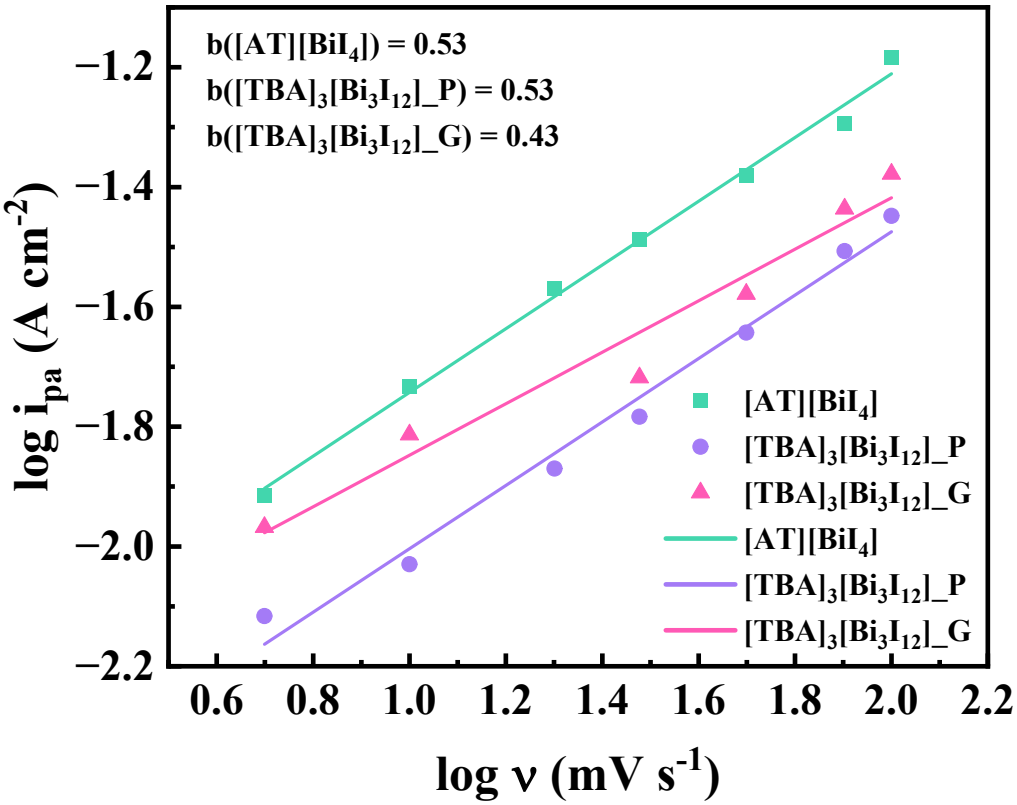

Figure S10 Plot between logarithm of anodic peak current density versus logarithm of scan rate

The relationship between current density and scan rate follows the formula 14:

$$i = av^b \quad \text{(Formula 14)}$$

Where a and b are constants, and the b value shows charge storage kinetics. When b = 0.5, it shows the process is diffusion-controlled, while b = 1 corresponds to surface-controlled process. The b values are always determined by plotting the logarithm of the peak current density (i_{pa}) versus the logarithm of scan rate (v), as shown in Fig S10. The calculated b values of three materials indicate that they are dominant by diffusion-controlled behaviour rather than only surface-controlled during charge and discharge, which demonstrates as battery-type electrodes.

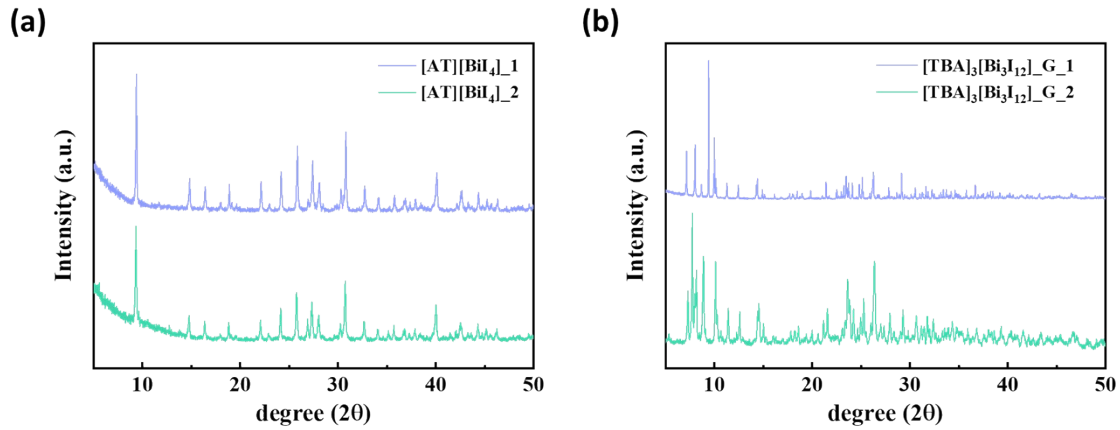

Figure S11 PXRD patterns of (a) $[AT][BiI_4]$ and (b) $[TBA]_3[Bi_3I_{12}]$_G from repeated syntheses, demonstrating the reproducibility of the materials.

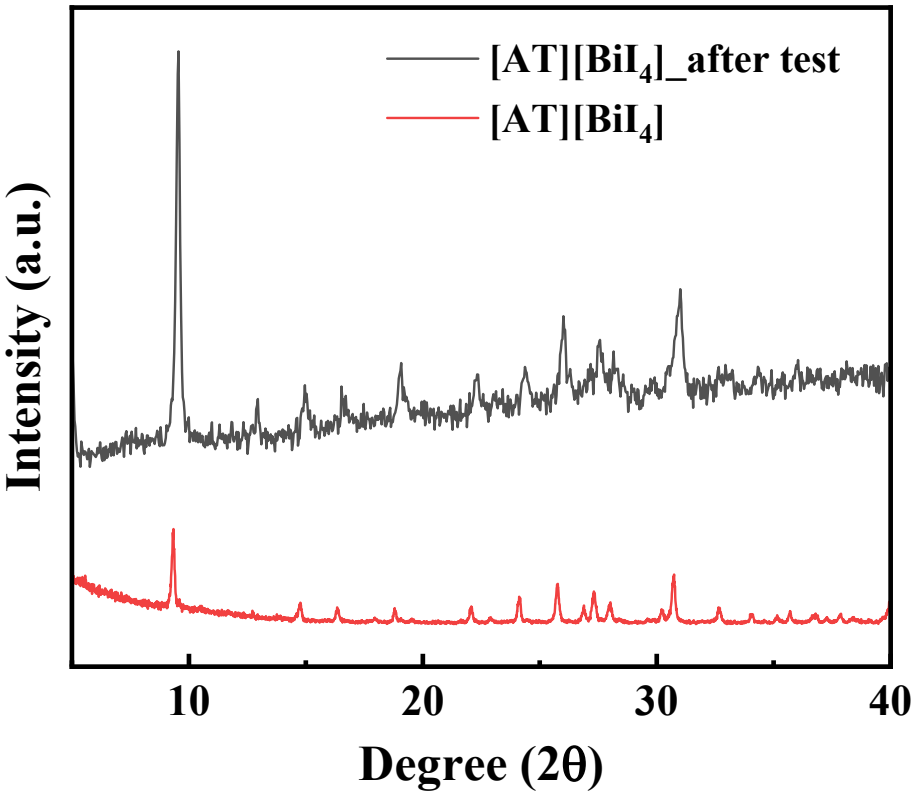

Figure S12 PXRD patterns of [AT][BiI_4] powder and the electrode after electrochemistry test, demonstrating the stability of [AT][BiI_4] in 1M KOH electrolyte.